23. M. Bose, C. Floss, F. J. Stadermann, R. M. Stroud, A. K. Speck, *Geochim. Cosmochim. Acta* **93**, 77–101 (2012).
24. A. N. Nguyen, L. R. Nittler, F. J. Stadermann, R. M. Stroud, C. M. O. Alexander, *Astrophys. J.* **719**, 166–189 (2010).
25. C. Vollmer, P. Hoppe, F. J. Stadermann, C. Floss, F. E. Brenker, *Geochim. Cosmochim. Acta* **73**, 7127–7149 (2009).
26. C. Floss, F. J. Stadermann, *Meteorit. Planet. Sci.* **47**, 992–1009 (2012).
27. C. Floss, F. Stadermann, *Geochim. Cosmochim. Acta* **73**, 2415–2440 (2009).
28. X. Zhao, C. Floss, Y. Lin, M. Bose, *Astrophys. J.* **769**, 49 (2013).
29. J. K. Hillier *et al.*, *Planet. Space Sci.* **97**, 9–22 (2014).
30. H. Kimura, *Mon. Not. R. Astron. Soc.* **449**, 2250–2258 (2015).
31. J. Slavin, P. Frisch, J. Heerikhuisen, N. Pogorelov, H. R. Mueller, W. T. Reach, G. Zank, A. Li, 38th COSPAR Scientific Assembly, Plenary Meeting (Bremen, Germany, 18 to 25 July 2010), p. 1618.
32. J. D. Slavin *et al.*, *Astrophys. J.* **760**, 46 (2012).
33. V. J. Sterken, P. Strub, H. Krüger, R. von Steiger, P. Frisch, *Astrophys. J.* **812**, 141 (2015).
34. J. D. Slavin, P. C. Frisch, *Astron. Astrophys.* **491**, 53–68 (2008).
35. J. M. Greenberg, J. I. Hage, *Astrophys. J.* **361**, 260 (1990).
36. H. Kimura, I. Mann, E. K. Jessberger, Meteoroids 2001 Conference, B. Warmbein, ed. (2001), vol. 495 of ESA Special Publication, pp. 633–642.
37. P. C. Frisch, J. D. Slavin, *Earth Planets Space* **65**, 175–182 (2013).
38. A. J. Westphal *et al.*, *Meteorit. Planet. Sci.* **49**, 1720–1733 (2014).
39. A. J. Westphal *et al.*, *Science* **345**, 786–791 (2014).
40. J. Leitner, C. Vollmer, P. Hoppe, J. Zipfel, *Astrophys. J.* **745**, 38 (2012).
41. J. P. Bradley *et al.*, *Science* **285**, 1716–1718 (1999).
42. L. P. Keller, S. Messenger, *Geochim. Cosmochim. Acta* **75**, 5336–5365 (2011).

ACKNOWLEDGMENTS

N.A. and F.P. acknowledge European Space Agency faculty funding for travels and meetings that were necessary for the completion of this work. Funding through Deutsche Forschungsgemeinschaft (DFG) within the priority program 1385 "The First 10 Million Years of the Solar System - A Planetary Materials Approach" is acknowledged by K.F., J.B. (grant BL 298/20-2), and R.S., M.T., E.G., J.H., and F.P. (grants TR333/14 and SR77/1). J.H. has received funding from the People Programme (Marie Curie Actions) of the European Union's Seventh Framework Programme FP7 2013 under Reemployment and Eligibility Assessment (REA) grant agreement number 622856. R.S. and F.P. acknowledge funding through Deutsches Zentrum für Luft- und Raumfahrt (DLR), Germany. V.J.S. acknowledges funding through the International Space Science Institute. N.K. acknowledges funding through the DFG. M.T. acknowledges funding by the Klaus Tschira Foundation. We thank J. Leitner, A. Westphal, R. Stroud, L. Nittler, P. Hoppe, H. Ishii, and H.-P. Gail for helpful discussions. We thank three anonymous reviewers for their thorough review of this paper. All CDA data used for this analysis are archived on the Small Bodies Node of the Planetary Data System (PDS-SBN), at http://sbn.psi.edu/archive/cocda.

SUPPLEMENTARY MATERIALS

www.sciencemag.org/content/352/6283/312/suppl/DC1
Materials and Methods
Figs. S1 to S6
Table S1
References (*43*–*61*)

3 June 2015; accepted 3 March 2016
10.1126/science.aac6397

REPORTS

MOLECULAR MAGNETISM

Magnetic remanence in single atoms

F. Donati,[1] S. Rusponi,[1] S. Stepanow,[2] C. Wäckerlin,[1] A. Singha,[1] L. Persichetti,[2] R. Baltic,[1] K. Diller,[1] F. Patthey,[1] E. Fernandes,[1] J. Dreiser,[1,3] Ž. Šljivančanin,[4,5] K. Kummer,[6] C. Nistor,[2] P. Gambardella,[2]* H. Brune[1]*

A permanent magnet retains a substantial fraction of its saturation magnetization in the absence of an external magnetic field. Realizing magnetic remanence in a single atom allows for storing and processing information in the smallest unit of matter. We show that individual holmium (Ho) atoms adsorbed on ultrathin MgO(100) layers on Ag(100) exhibit magnetic remanence up to a temperature of 30 kelvin and a relaxation time of 1500 seconds at 10 kelvin. This extraordinary stability is achieved by the realization of a symmetry-protected magnetic ground state and by decoupling the Ho spin from the underlying metal by a tunnel barrier.

The search for the ultimate size limit of magnetic information storage, and the aim of exploring magnetic quantum properties for information processing, have driven fundamental research toward atomic-scale structures that contain fewer and fewer atoms. Benchmarks for such systems are long magnetic relaxation times, i.e., magnetic quantum states that are stable on the time scales required for storage or quantum computation. Single-molecule magnets (*1*–*6*) are promising candidates as they are chemically robust in ambient conditions and exhibit magnetic bistability at cryogenic temperatures, with a record relaxation time of 100 s at 13.9 K for N_2^{3-} radical-bridged dilanthanide complexes in the bulk phase (*6*). Further reducing the number of constituent atoms in such systems, however, implies removing the organic ligands, thereby bringing the magnetic core in direct contact with a surface. Presently, the smallest magnets are antiferromagnetic Fe_{12} double chains (*7*) and ferromagnetic Fe_5 clusters (*8*) supported on nonmagnetic surfaces. Both exhibit lifetimes of hours below 0.5 K, while supported nanostructures of smaller size retain their magnetic orientation only on a time scale of seconds (*9*, *10*).

Ultimately, the smallest size of a magnet can be reached with a single surface-adsorbed atom. The magnetism of single atoms has become the subject of intense research (*11*–*17*) since the discovery of a giant magnetic anisotropy for Co atoms adsorbed onto a Pt(111) surface (*18*). However, despite the high magnetic anisotropy originating from the extremely low coordination, all adatom-surface combinations investigated so far are paramagnetic down to 0.3 K, with the longest achieved magnetic lifetime being 230 μs at 0.6 K (*16*, *17*). Thus, in addition to anisotropy, the magnetic states of a quantum magnet need to be protected from quantum tunneling of the magnetization as well as from scattering with electrons and phonons of the substrate. The first condition requires a degenerate ground state doublet with a projected total angular momentum J_z that is protected from mixing with other states by the symmetry of the adsorption sites' ligand field (*19*, *20*). The second requires decoupling the magnetic atom from the phonon and conduction electron baths.

Here, we investigated ensembles of rare-earth atoms, whose spin and orbital moments originate from the strongly localized 4f orbitals and interact weakly with the surrounding environment. Additional decoupling is ensured by choosing an insulating substrate with low phonon density of states, such as MgO. We found that Ho atoms deposited on MgO(100) thin films grown on a Ag(100) surface formed single-atom magnets with a relaxation time that depended on the MgO thickness. Not only did the Ho atoms show magnetic bistability, they also had exceptionally large coercive field and showed magnetic hysteresis up to 30 K, a temperature substantially higher than the blocking temperature of single-molecule magnets on comparable time scales. These exceptional properties originate from a combination of factors—namely, the specific mixing of odd J_z states of Ho in the C_{4v} symmetric ligand field of MgO(100), which protects the magnetization from reversal by tunneling and first-order electron scattering at zero and finite fields, and the weak coupling to the electronic and vibrational degrees of freedom of the substrate, provided by the stiff and insulating MgO buffer layer.

We created a quasi-monodisperse ensemble of individual Ho atoms adsorbed on ultrathin MgO(100) films grown on Ag(100) by depositing minute amounts of Ho at a sample temperature below 10 K, which ensured that the thermal mobility of the adatoms was blocked. Low-temperature scanning tunneling microscopy (STM) images

[1]Institute of Physics, Ecole Polytechnique Fédérale de Lausanne (EPFL), Station 3, CH-1015 Lausanne, Switzerland. [2]Department of Materials, ETH Zürich, Hönggerbergring 64, CH-8093 Zürich, Switzerland. [3]Swiss Light Source, Paul Scherrer Institute, CH-5232 Villigen PSI, Switzerland. [4]Vinča Institute of Nuclear Sciences (020), Post Office Box 522, 11001 Belgrade, Serbia. [5]Texas A&M University at Qatar, Doha, Qatar. [6]European Synchrotron Radiation Facility (ESRF), F-38043 Grenoble, France.
***Corresponding author. E-mail: pietro.gambardella@mat.ethz.ch (P.G.); harald.brune@epfl.ch (H.B.)**

displayed the Ho atoms as localized protrusions with identical apparent heights and widths (Fig. 1A). Ab initio calculations using density functional theory (DFT) in the GGA+U approximation (*21*) identify the O-top as the most favorable adsorption site (Fig. 1B and table S3). Atomic-resolution images of samples with coadsorbed Co or Fe atoms confirmed this assignment (fig. S2). The adatoms were immobile up to 50 K and, therefore, at all temperatures where we characterized their magnetic properties.

X-ray absorption and magnetic circular dichroism spectra (XAS and XMCD) taken at the Ho $M_{4,5}$ edges (3d→4f transitions) with the x-ray beam and magnetic field parallel to the surface normal revealed a pronounced dichroism (Fig. 1D). This magnetic signal indicates the presence of a large localized magnetic moment that aligns along the field direction. Recording the maximum of the XMCD peak as a function of the external field allowed us to measure the magnetization loop of the Ho adatoms. At 6.5 K, we observed a clear hysteresis opening along the out-of-plane direction and a remanent magnetization of 25% of saturation (Fig. 1E). After saturation, the Ho atoms retained their magnetization even in the absence of an external field. In addition, the loop showed a coercive field of 1 T and remains open up to the maximum available field of 8.5 T, indicating a long relaxation time even at extremely high magnetic fields.

This exceptional magnetic stability is related to the symmetry of the Ho quantum states. We identify them by comparing experimental spectra and magnetization curves with multiplet calculations (fig. S6). At zero field, the ground state is a perfectly degenerate doublet. The two states, labeled as $|0\rangle$ and $|1\rangle$, exhibited out-of-plane projections of the total moment $\langle J_z = \pm 4.66 \rangle$ (Fig. 1C). This value matches well with the result of the sum rules directly applied to the experimental XAS and XMCD spectra (*22*). In the C_{4v} symmetry of the O adsorption site, this ground state doublet is a superposition of the the quantum states $J_z = \pm 7; \pm 3; \mp 1$; and ∓ 5, with the first two contributing the most (table S2). Thus, it is protected from first-order spin excitations ($\Delta m = 0, \pm 1$) at any external magnetic field (*20*), which prevents magnetization reversal by electron scattering. In addition, the very low density of vibrational modes in the MgO layer (fig. S9) strongly suppresses first-order scattering with phonons ($\Delta m = \pm 1, \pm 2$). The absence of Ho-MgO vibrational modes in the region of hyperfine level crossing can further slow down relaxation at low fields, as observed for $TbPc_2$ molecules grafted on suspended nanotubes (*23*). Thus, the combination of magnetic ground state, symmetry of the adsorption site, and decoupling from the metal substrate guarantees protection against all first-order scattering and ultimately allows for long magnetic lifetimes.

The first excited state $|2\rangle$ is a $\langle J_z = 0 \rangle$ singlet lying 4.5 meV above the ground state. This energy separation is sufficient to prevent electronic level crossings up to more than 10 T (Fig. 1C), hence the absence of quantum tunneling steps in the hysteresis loop (*3*). Further excited states lie at a higher energy and played no role at the temperatures and magnetic fields used here.

To access the magnetic lifetime, we first initialized the ensemble of Ho atoms in the $|0\rangle$ state by applying an external field B = +6.8 T until saturation was reached. We then swept the magnetic field to near zero (B = 0.01 T) and recorded the time needed for the magnetization of the ensemble to vanish—namely, to reach equal occupation of the $|0\rangle$ and $|1\rangle$ states (Fig. 2A). At a temperature of 10 K, we found an exponential decrease in the XMCD signal with a characteristic lifetime of τ = 1586 ± 131 s (Fig. 2C). Notably, we observed comparable magnetic lifetimes down to 2.5 K (fig. S4A), implying that below 10 K, the magnetic relaxation is essentially driven by nonthermal processes.

Measurements at different photon fluxes revealed that the lifetime of Ho atoms is mostly limited by the secondary electron cascade generated by the absorbed photons. The scattering with these hot electrons reduces the magnetic lifetime, as recently reported for endofullerene single-molecule magnets (*24*). The measured lifetimes hence represent a lower bound to the intrinsic magnetic lifetimes. Extrapolation to the zero-flux limit suggests intrinsic lifetimes of the order of 1 hour at 2.5 K (fig. S4B). Increasing the temperature to 20 K activates thermal relaxation processes and results in a slightly decreased magnetic lifetime of 675 ± 77 s (Fig. 2C). The lifetime of the Ho atoms on MgO is much longer than for Ho

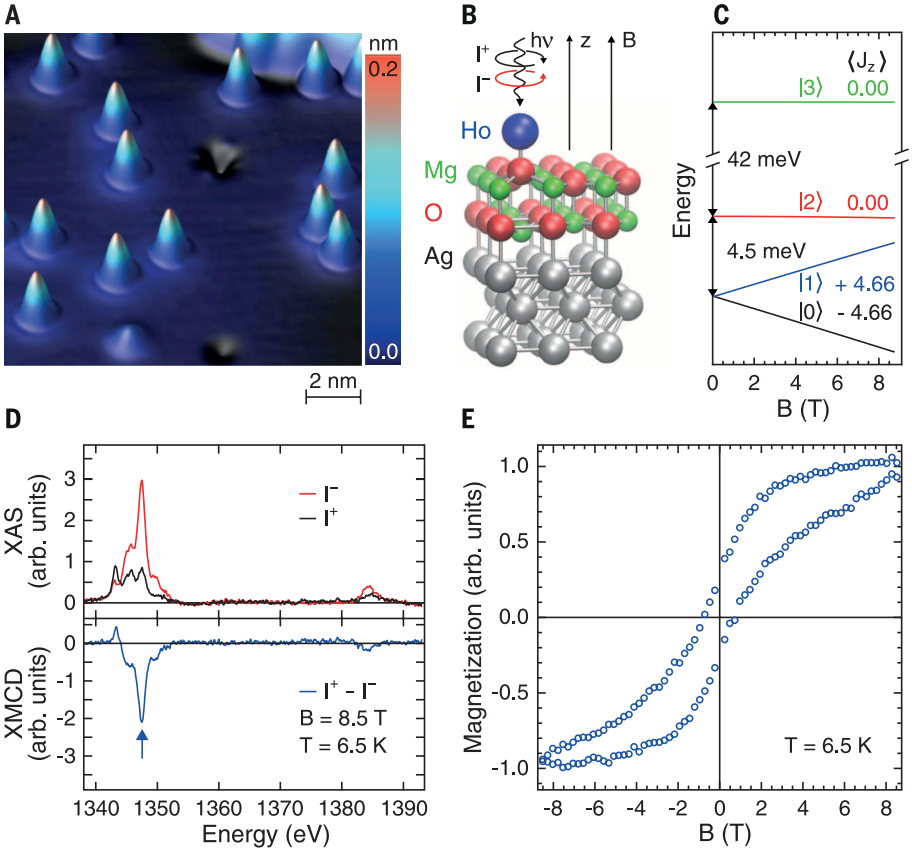

Fig. 1. Ho atoms on MgO films. (**A**) Constant-current STM image of Ho atoms on 2 monolayer (ML) MgO/Ag(100) (tunnel voltage V_t = 100 mV, tunnel current I_t = 20 pA, T = 4.7 K, Ho coverage Θ_{Ho} = 0.005 ± 0.001 ML). (**B**) Adsorption geometry of Ho atoms on top of O on 2-ML MgO/Ag(100) as simulated with DFT, together with a schematic of the XAS experiment. (**C**) Splitting of the lowest quantum levels of Ho atoms from multiplet calculations. Zero-field values of $\langle J_z \rangle$ are reported. (**D**) XAS and XMCD at the $M_{4,5}$ edges for an ensemble of individual Ho adatoms. The arrow points to the maximum of the XMCD signal that is recorded as a function of magnetic field to obtain the magnetization curves shown in (**E**) (field sweep rate dB/dt) = 8 mT/s, photon flux $\phi = 1 \times 10^{-2}$ nm^{-2} s^{-1}, T = 6.5 K, Θ_{Ho} = 0.01 ML, MgO coverage Θ_{MgO} = 7.0 ML).

ions in $HoPc_2$ (*25*) and Ho-doped bulk crystals (*26*), possibly because of the larger level splitting and the smaller number of vibration modes allowed for atoms adsorbed on surfaces.

We further characterized the magnetic lifetime at a large magnetic field. We prepared the ensemble in the $|1\rangle$ state at $B = -6.8$ T and measured the time needed to fully reverse to the $|0\rangle$ state at $B = +6.8$ T and $T = 10$ K (Fig. 2B). We observed an exponential increase in the magnetization up to saturation with $\tau_{rev} = 1223 \pm 69$ s (Fig. 2D). Thus, the Ho atoms on MgO retained their long lifetimes even at a very high field where single-molecule magnets typically exhibit faster relaxations because of level crossing, quantum tunneling of the magnetization, or scattering with phonons (*1*–*5*).

To probe the temperature dependence of the remanence and of the coercive field of Ho atoms, we recorded hysteresis loops in the most favorable experimental conditions, i.e., using the fastest field sweep rate dB/dt and lowest photon flux achievable (Fig. 3A). Under these conditions, the hysteresis opening at 10 K (Fig. 3B) was even wider than the one in Fig. 1E, showing a coercive field of 3.7 ± 0.3 T and a remanent magnetization of 50% of saturation. In addition, the hysteresis remained open up to 30 K, and only at 40 K was the magnetization loop essentially closed (Fig. 3C). These results further show that the magnetic quantum states of Ho atoms were notably protected against scattering with Ag conduction electrons and MgO phonons.

Although the Ho ground state was protected against magnetization reversal via first-order electron-spin excitations, it is possible, in principle, to reverse the magnetization via direct scattering with phonons or by two-electron or -phonon transitions through the first excited state. The reversal processes that are triggered by the scattering with conduction electrons and with the soft phonon modes of the underlying metal are expected to critically depend on the thickness of the MgO layer. Accordingly, we observed that the hysteresis loops of Ho atoms became narrower when the thickness of

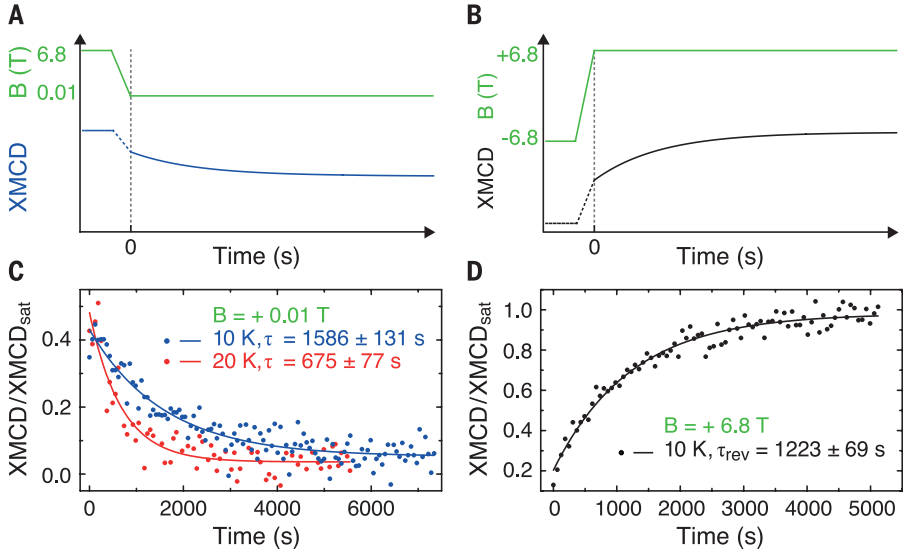

Fig. 2. Magnetization lifetime. (**A** and **B**) Scheme of the measurements. After saturation at $|B_{max}| = 6.8$T, the field was swept to the indicated values. Measurements of XMCD started at the end of the sweep. (**C** and **D**) Time evolution of the maximum XMCD intensity (dots) normalized to the saturation value at $B = +6.8$ T ($\Theta_{Ho} = 0.015$ ML, $\Theta_{MgO} = 6.0$ ML, $\phi = 0.14 \times 10^{-2}$ nm^{-2} s^{-1}, $dB/dt = 33$ mT/s). Exponential fits (solid lines) give the magnetic lifetime τ and reversal time τ_{rev} of the Ho atoms.

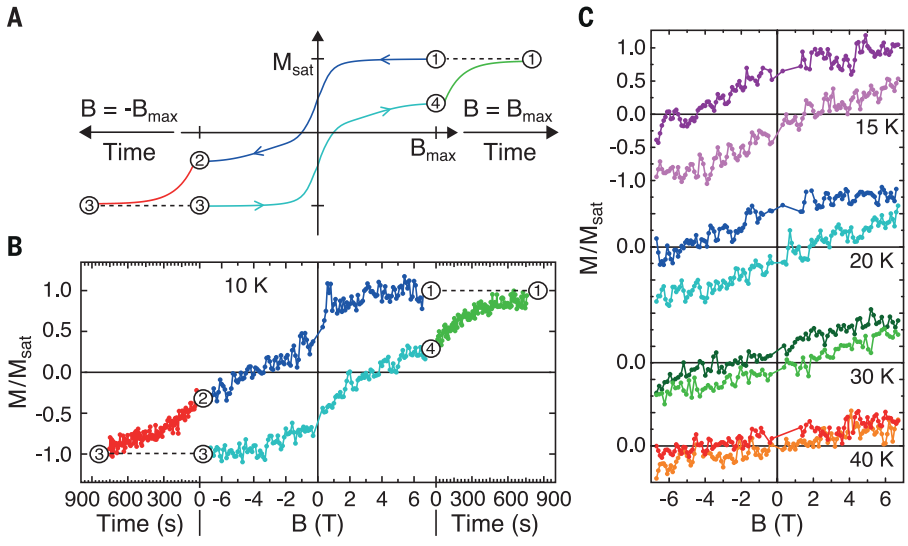

Fig. 3. Magnetic hysteresis at increasing temperatures. (**A**) Scheme for the hysteresis measurements at a fast sweep rate of the magnetic field. We first kept the magnetic field at $+B_{max}$ for sufficient time to reach $+M_{sat}$ (*1*), then measured M while sweeping the field to $-B_{max}$ (*2*). This fast sweep leaves the system out of equilibrium at B_{max}. Thus, we allow the system to relax at constant $B = -B_{max}$ until equilibrium is reached (*3*) before starting the new branch of the loop (3-4-1). (**B**) Hysteresis loop recorded at $T = 10$ K following the scheme described in (A). (**C**) Evolution of the hysteresis loop with the temperature (dark, downsweep; light, upsweep). The relaxation part is not shown ($\Theta_{Ho} = 0.01$ ML, $\Theta_{MgO} = 4.3$ ML, $\phi = 0.55 \times 10^{-2}$ nm^{-2} s^{-1}, $dB/dt = 33$ mT/s).

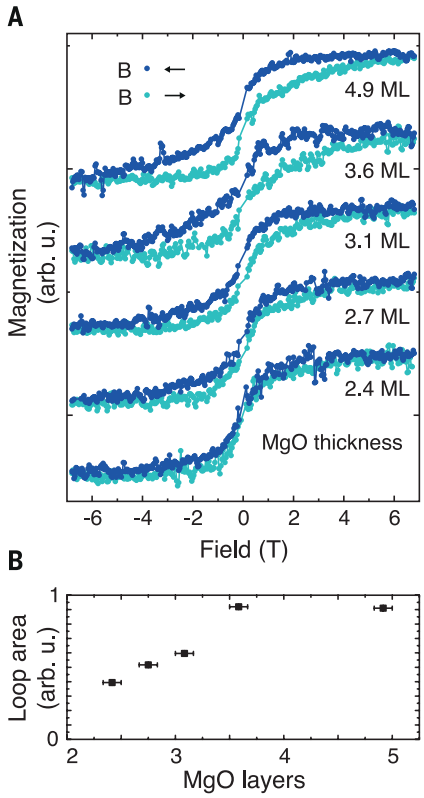

Fig. 4. Effect of the MgO layer thickness. (**A**) Magnetization loops acquired on Ho atoms on MgO films of various thicknesses as indicated close to each loop ($T = 2.5$ K, $dB/dt = 12$ mT/s, $\phi = 2.15 \times 10^{-2}$ nm^{-2} s^{-1}, $\Theta_{Ho} = 0.005$ to 0.010 ML). The curves were rescaled to the corresponding saturation value at $B = +6.8$ T. The reduced loop opening compared to that in Figs. 1 and 3 is a consequence of the higher photon flux and the lower sweep rate used here. (**B**) Loop area as a function of MgO thickness, reaching a constant value at 3.6 ML.

the MgO film was reduced below 3.6 monolayers (ML) and were almost closed for a thickness of 2.4 ML (Fig. 4). We observed essentially no variation in the XAS and XMCD spectra of Ho atoms with the number of MgO layers (fig. S5), hence the Ho ground state was unaffected by the MgO thickness. Thus, protection against first-order reversal is a necessary but not a sufficient condition to prevent magnetization reversal. To obtain long magnetic lifetimes in single atoms, an efficient decoupling from the electron and phonon bath is also required to ultimately suppress higher-order scattering processes that cannot be eliminated by symmetry. This result also suggests that long spin lifetimes are unlikely for single atoms in direct contact with a metal substrate.

The need of a decoupling layer to obtain long lifetimes is in stark contrast with the interpretation of STM experiments on Ho atoms on Pt(111), which reported telegraph noise in the differential conductance with characteristic times of up to 700 s at T = 0.7 K and zero field (*19*). This signal was interpreted as magnetic bistability and ascribed to a J_z = 8 ground state, as calculated by DFT, which would be protected by the C_{3v} symmetry of the adsorption site. However, XMCD measurements revealed that Ho atoms on Pt(111) have a ground state J_z = 6 that is incompatible with long spin lifetimes in a C_{3v}-symmetric crystal field (*27*). In addition, the magnetization curves at 2.5 K are fully reversible. According to these XMCD results, Ho/Pt(111) is a perfect paramagnet, as are all the other single atoms on surfaces previously reported. Moreover, subsequent STM experiments on the same system could reproduce neither telegraph noise nor spin excitations (*10*). Together with further STM observations on other 4f elements (*28*), this questions the interpretation of the results reported in (*19*) as magnetic bistability of Ho/Pt(111).

The relative simplicity of the Ho/MgO system, based on common physical deposition methods, as well as the planar geometry of the system opens the possibility of probing and manipulating the Ho spin and its environment in a controlled way. Using MgO as a decoupling layer could improve the magnetic stability not only of individual atoms but also of surface-supported molecular magnets, paving the road to scalable and robust nanoscale spintronic devices.

REFERENCES AND NOTES

1. R. Sessoli, D. Gatteschi, A. Caneschi, M. A. Novak, *Nature* **365**, 141–143 (1993).
2. N. Ishikawa, M. Sugita, T. Ishikawa, S. Y. Koshihara, Y. Kaizu, *J. Am. Chem. Soc.* **125**, 8694–8695 (2003).
3. M. Mannini *et al*., *Nature* **468**, 417–421 (2010).
4. J. M. Zadrozny *et al*., *Nat. Chem.* **5**, 577–581 (2013).
5. L. Ungur, J. J. Le Roy, I. Korobkov, M. Murugesu, L. F. Chibotaru, *Angew. Chem. Int. Ed.* **53**, 4413–4417 (2014).
6. J. D. Rinehart, M. Fang, W. J. Evans, J. R. Long, *J. Am. Chem. Soc.* **133**, 14236–14239 (2011).
7. S. Loth, S. Baumann, C. P. Lutz, D. M. Eigler, A. J. Heinrich, *Science* **335**, 196–199 (2012).
8. A. A. Khajetoorians *et al*., *Science* **339**, 55–59 (2013).
9. S. Yan, D.-J. Choi, J. A. J. Burgess, S. Rolf-Pissarczyk, S. Loth, *Nat. Nanotechnol.* **10**, 40–45 (2015).
10. M. Steinbrecher *et al*., *Nat. Commun.* **7**, 10454 (2016).
11. C. F. Hirjibehedin *et al*., *Science* **317**, 1199–1203 (2007).
12. F. Meier, L. Zhou, J. Wiebe, R. Wiesendanger, *Science* **320**, 82–86 (2008).
13. H. Brune, P. Gambardella, *Surf. Sci.* **603**, 1812–1830 (2009).
14. A. A. Khajetoorians *et al*., *Phys. Rev. Lett.* **106**, 037205 (2011).
15. F. Donati *et al*., *Phys. Rev. Lett.* **111**, 236801 (2013).
16. I. G. Rau *et al*., *Science* **344**, 988–992 (2014).
17. S. Baumann *et al*., *Science* **350**, 417–420 (2015).
18. P. Gambardella *et al*., *Science* **300**, 1130–1133 (2003).
19. T. Miyamachi *et al*., *Nature* **503**, 242–246 (2013).
20. C. Hübner, B. Baxevanis, A. A. Khajetoorians, D. Pfannkuche, *Phys. Rev. B* **90**, 155134 (2014).
21. P. Blaha, K. Schwarz, G. Madsen, D. Kvasnicka, J. Luitz, WIEN2k: An Augmented Plane Wave plus Local Orbitals Program for Calculating Crystal Properties (Karlheinz Schwarz, Techn. Universitat Wien, Austria, 2001).
22. Supplementary materials are available on *Science* Online.
23. M. Ganzhorn, S. Klyatskaya, M. Ruben, W. Wernsdorfer, *Nat. Nanotechnol.* **8**, 165–169 (2013).
24. J. Dreiser *et al*., *Appl. Phys. Lett.* **105**, 032411 (2014).
25. N. Ishikawa, M. Sugita, W. Wernsdorfer, *J. Am. Chem. Soc.* **127**, 3650–3651 (2005).
26. R. Giraud, W. Wernsdorfer, A. M. Tkachuk, D. Mailly, B. Barbara, *Phys. Rev. Lett.* **87**, 057203 (2001).
27. F. Donati *et al*., *Phys. Rev. Lett.* **113**, 237201 (2014).
28. D. Coffey *et al*., *Sci. Rep.* **5**, 13709 (2015).

ACKNOWLEDGMENTS

Funding from the Swiss National Science Foundation (grants 200021-153404, 200020-157081, 200021-146715, PZ00P2 142474, and IZ73Z0-152406) and the Swiss Competence Centre for Materials Science and Technology (CCMX) is gratefully acknowledged. L.P. was supported by an ETH Postdoctoral Fellowship (FEL-42 13-2). K.D. acknowledges support from the "EPFL Fellows" fellowship program cofunded by Marie Curie, FP7 grant agreement no. 291771. Z.S. was supported by the Serbian Ministry of Education and Science under grants ON171033 and ON171017. The DFT calculations were performed at the PARADOX-IV supercomputer at the Scientific Computing Laboratory (SCL) of the Institute of Physics Belgrade. The XMCD experiments were performed at the EPFL-PSI X-Treme beamline of the Swiss Light Source (SLS) and the ID32 beamline of the European Synchrotron Radiation Facility (ESRF). The authors declare that they have no competing financial interests.

SUPPLEMENTARY MATERIALS

www.sciencemag.org/content/352/6283/318/suppl/DC1
Materials and Methods
Figs. S1 to S9
Tables S1 to S3
References (*29*–*56*)

4 December 2015; accepted 8 March 2016
10.1126/science.aad9898

HYDROGEN BONDING

Nuclear quantum effects of hydrogen bonds probed by tip-enhanced inelastic electron tunneling

Jing Guo,[1]* Jing-Tao Lü,[2]* Yexin Feng,[1,3]* Ji Chen,[1] Jinbo Peng,[1] Zeren Lin,[1] Xiangzhi Meng,[1] Zhichang Wang,[1] Xin-Zheng Li,[4,5]† En-Ge Wang,[1,5]† Ying Jiang[1,5]†

We report the quantitative assessment of nuclear quantum effects on the strength of a single hydrogen bond formed at a water-salt interface, using tip-enhanced inelastic electron tunneling spectroscopy based on a scanning tunneling microscope. The inelastic scattering cross section was resonantly enhanced by "gating" the frontier orbitals of water via a chlorine-terminated tip, so the hydrogen-bonding strength can be determined with high accuracy from the red shift in the oxygen-hydrogen stretching frequency of water. Isotopic substitution experiments combined with quantum simulations reveal that the anharmonic quantum fluctuations of hydrogen nuclei weaken the weak hydrogen bonds and strengthen the relatively strong ones. However, this trend can be completely reversed when a hydrogen bond is strongly coupled to the polar atomic sites of the surface.

In terms of tunneling and zero-point motion, nuclear quantum effects (NQEs) play important roles in the structure, dynamics, and macroscopic properties of hydrogen-bonded (H-bonded) materials (*1*–*5*). Despite enormous theoretical efforts toward pursuing proper treatment of the nuclear motion at a quantum mechanical level (*5*–*9*), accurate and quantitative description of NQEs on the H-bonding interaction has proven to be experimentally challenging. Conventional methods for probing the NQEs are based on spectroscopic or diffraction techniques (*4*, *10*–*14*). However, those techniques have poor spatial resolution and only measure the average properties of many H bonds, which are susceptible to structural inhomogeneity and local environments. The spatial variation and interbond coupling of H bonds lead to spectral broadening that may easily smear out the subtle details of NQEs.

[1]International Center for Quantum Materials, School of Physics, Peking University, Beijing 100871, P. R. China. [2]School of Physics and Wuhan National High Magnetic Field Center, Huazhong University of Science and Technology, Wuhan 430074, P. R. China. [3]School of Physics and Electronics, Hunan University, Changsha 410082, P. R. China. [4]School of Physics, Peking University, Beijing 100871, P. R. China. [5]Collaborative Innovation Center of Quantum Matter, Beijing 100871, P. R. China.
*These authors contributed equally to this work. **†Corresponding author. E-mail: xzli@pku.edu.cn (X.-Z.L.); egwang@pku.edu.cn (E.-G.W.); yjiang@pku.edu.cn (Y.J.)**